Journal of Solid State Chemistry 188 (2012) 77–83

Contents lists available at SciVerse ScienceDirect

Journal of Solid State Chemistry

journal homepage: www.elsevier.com/locate/jssc

New metal-organic frameworks of $[M(C_6H_5O_7)(C_6H_6O_7)(C_6H_7O_7)(H_2O)] \cdot H_2O$ (M=La, Ce) and $[Ce_2(C_2O_4)(C_6H_6O_7)_2] \cdot 4H_2O$

Sheng-Feng Weng, Yun-Hsin Wang, Chi-Shen Lee *

Department of Applied Chemistry, National Chiao Tung University, 1001 University Rd., Hsinchu 30010, Taiwan

ARTICLE INFO

Article history:
Received 11 October 2011
Received in revised form
12 January 2012
Accepted 23 January 2012
Available online 31 January 2012

Keywords:
Rare earth
Copper
Citric acid
Oxalate
Hydrothermal
Metal organic framework

ABSTRACT

Two novel materials, $[M(C_6H_5O_7)(C_6H_6O_7)(C_6H_7O_7)(H_2O)] \cdot H_2O$ (M=La(**1a**), Ce(**1b**)) and $[Ce_2(C_2O_4)(C_6H_6O_7)_2] \cdot 4H_2O$ (**2**), with a metal-organic framework (MOF) were prepared with hydrothermal reactions and characterized with photoluminescence, magnetic susceptibility, thermogravimetric analysis and X-ray powder diffraction *in situ*. The crystal structures were determined by single-crystal X-ray diffraction. Compound **1** crystallized in triclinic space group $P\bar{1}$ (No. 2); compound **2** crystallized in monoclinic space group $P2_1/c$ (No. 14). The structure of **1** is built from a 1D MOF, composed of deprotonated citric ligands of three kinds. Compound **2** contains a 2D MOF structure consisting of citrate and oxalate ligands; the oxalate ligand arose from the decomposition *in situ* of citric acid in the presence of Cu^{II} ions. Photoluminescence spectra of compounds **1b** and **2** revealed transitions between the $5d^1$ excited state and two levels of the $4f^1$ ground state ($^2F_{5/2}$ and $^2F_{7/2}$). Compounds **1b** and **2** containing Ce^{III} ion exhibit a paramagnetic property with weak antiferromagnetic interactions between the two adjacent magnetic centers.

1. Introduction

Metal-organic frameworks (MOFs) that exhibit intriguing structural diversity have attracted considerable interest because of the flexible coordination environments of the metal ions to their ligands [1]. The structures and physical properties of MOFs can be modulated by the particular metal cations and ligands [2]. Their prospective applications include gas adsorption and storage [3], ion exchange [4], and catalysis [5]. For the diverse structures, the counter-anions [6], solvents [7], metal–ligand ratio [8], pH [9], and reaction temperature [10] are thought to be the notable factors to affect the frameworks obtained.

Many metal-carboxylate complexes with 1D, 2D or 3D structures have been discovered since year 2000 [11]. As a choice for a metal center, rare-earth ions are attractive for the synthesis of the new MOF because of the extended coordination numbers from *f*-block orbitals [12]. For the choice of anion ligands, multidentate ligands, such as citric acid of which a molecule contains a hydroxyl and three carboxylate groups to provide at least seven donor sites – one from an α-position hydroxyl group, two from an α-position carboxyl group and four from two β-position carboxyl groups – are capable of coordinating most metal ions to form coordination complexes of novel structural types. Many authors have reported research on MOF composed of carboxylate and varied metal ions, including main-group metal ions, Pb^{II} [13] and Bi^{III} [14], transition-metal ions Cd^{II} [15], Zn^{II}, Cu^{II} [16], and Co^{II}[17] and rare-earth metal cations [18]. Among these compounds, MOFs with transition-metal or rare-earth cations coordinated with citrate or oxalate ligands are well developed [19], but MOF built of citrate ligands with variably deprotonated modes or citrate/oxalate ligands are few [20]: only compound $Rb_2Sb_4(C_6H_5O_7)_2(C_6H_6O_7)_2(C_6H_7O_7)_4(H_2O)_2$ is known as a coordination polymer containing three separately deprotonated citrate ligands [21].

Our syntheses of new MOF using rare-earth cations with citrate ligand have enabled an assessment of the coordination capabilities; several new coordination polymers composed of La^{III} and Ce^{III} ions bound to citrate ligands in a separate deprotonated mode and citrate/oxalate ligands were prepared. Herein, we report the syntheses and characterization of three novel rare-earth MOF materials, $[M(C_6H_5O_7)(C_6H_6O_7)(C_6H_7O_7)(H_2O)] \cdot H_2O$ (**1a**:M=La, **1b**:M=Ce) and $[Ce_2(C_2O_4)(C_6H_6O_7)_2] \cdot 4H_2O$ (**2**). Under hydrothermal conditions, the deprotonated mode of the citrate ligands is controllable with the reaction temperature, and the decomposition *in situ* of citrate ligands to oxalate ligands is facilitated by the presence of Cu^{II} ions.

2. Experiments

2.1. General

All reactions were performed under hydrothermal conditions. The precursor chemicals (analytical grade, Aldrich and Alfa Aesar) were used without further purification. The elemental content of C, H, N (Heraeus CHN-O-S-Rapid analyzer), IR spectra (Perkin-Elmer,

* Corresponding author. Fax: +886 3 5723764.
E-mail address: chishen@mail.nctu.edu.tw (C.-S. Lee).

0022-4596/$ - see front matter © 2012 Elsevier Inc. All rights reserved.
doi:10.1016/j.jssc.2012.01.046

Spectrum One), differential thermal analysis (DTA) and thermogravimetric analysis (TG, NETZSCH STA 409PC thermal analyzer), photoluminescence spectra (Jobin-Yvon Spex Fluorolog-3, Xe lamp, 296 K, scanning wavelength 200–800 nm), magnetic properties (MPMS5 superconducting quantum- interference-device magnetometer, field 1000 Oe in temperature range 2–300 K) were measured with the indicated instruments.

2.1.1. Preparation of $[La_2(C_6H_5O_7)(C_6H_6O_7)(C_6H_7O_7)(H_2O)]\cdot H_2O$ (**1a**)

$La(NO_3)_3\cdot 6H_2O$ (1 mmol) and citric acid (0.02 mol) were added to DI water (16 mL) and stirred for 10 min. The clear solution was then transferred into an autoclave (20 mL, Telfon-lined). After the treatment under hydrothermal conditions at 150 °C for 48 h, transparent crystals of needle shape were isolated with a centrifuge, washed several times with DI water and dried at 50 °C. Elemental analysis: calcd (%) for $C_{18}H_{22}O_{23}La_2$: C, 24.43; H, 2.49. Found: C, 24.05; H, 2.25. IR (KBr, cm^{-1}): 3513, 3383, 3217, 2965, 2951, 1942, 1726, 1707, 1442, 1417, 1400, 1389, 1335, 1296, 1282, 1157, 1109, 1084, 1014, 951, 905, 839, 728, 620, 542.

2.1.2. Preparation of $[Ce_2(C_6H_5O_7)(C_6H_6O_7)(C_6H_7O_7)(H_2O)]\cdot H_2O$ (**1b**)

$Ce(NO_3)_3\cdot 6H_2O$ (1 mmol) and citric acid (0.02 mol) were added to DI water (16 mL) and stirred for 10 min. The clear solution was then transferred into an autoclave (20 mL, Telfon-lined). After the treatment under hydrothermal conditions at 150 °C for 48 h, transparent crystals of needle shape were isolated by centrifugation, washed several times with DI water and dried at 50 °C. Elemental analysis: calcd (%) for $C_{18}H_{22}O_{23}Ce_2$: C, 24.35; H, 2.48. Found: C, 24.22; H, 2.65. IR (KBr, cm^{-1}): 3508, 3392, 3211, 2966, 2949, 1936, 1726, 1708, 1443, 1416, 1401, 1388, 1335, 1296, 1282, 1158, 1109, 1084, 1015, 952, 905, 840, 728, 621, 543 for **1b**.

2.1.3. Preparation of $[Ce_2(C_2O_4)(C_6H_6O_7)_2]\cdot 4H_2O$ (**2**)

The hydrothermal treatment was similar to the synthesis of **1a**, except that compound **2** was obtained from a reaction with $Cu(NO_3)_2\cdot 3H_2O$, $Ce(NO_3)_3\cdot 6H_2O$, and citric acid in molar ratio of 1:2:40. The product consisted of colorless plate-shaped crystals and a small amount of black powder. Elemental analysis: calcd (%) for $C_7H_{10}O_{11}Ce$: C, 20.47; H, 2.44. Found: C, 19.72; H, 2.34. IR (KBr, cm^{-1}): 3518, 3407, 3206, 2984, 2946, 2024, 1700, 1432, 1406, 1383, 1322, 1269, 1246, 1195, 1145, 1061, 958, 938, 901, 855, 837, 801, 749, 619, 554, 503.

2.2. Characterization

2.2.1. Single-crystal X-ray diffraction (XRD)

Single crystals of compounds **1a** ($0.1\times0.2\times1.6\ mm^3$) and **2** ($0.2\times0.4\times0.5\ mm^3$) were mounted on a glass fiber with epoxy glue; intensity data were collected at 298 K on a diffractometer (Bruker APEX CCD) equipped with graphite-monochromated Mo-$K\alpha$ radiation ($\lambda=0.71073$ Å) at 298(2) K. The distance from the crystal to the detector was 5.038 cm. Data were collected in scans of 0.3° in groups of 600 frames each at ϕ settings 0°, 90°, 180°, and 270°. The exposure duration was 45 and 40 s/frame for **1a** and **2**, respectively. The 2θ values varied between 3.06° and 56.58° for **1a** and between 6.02° and 57.20° for **2**. The unit-cell parameters were determined from diffraction signals obtained from all frames of reciprocal-space images. The data were integrated (Siemens SAINT program) and corrected for Lorentz and polarization effects.[22] Absorption corrections were based on fitting a function to the empirical transmission surface as sampled with multiple equivalent measurements of numerous reflections. The structural model was obtained through direct methods and refined with full-matrix least-square refinement based on F^2 (SHELXTL package) [23]. Data for the crystal structures of compounds **1a** to **2** have been allocated accession numbers CCDC 837058 and 837059 at the Cambridge Crystallographic Data Centre; these data are obtainable free of charge via Internet at ww.ccdc.cam.ac.uk/conts/retrieving.html.

2.2.2. Powder X-ray diffraction in situ

Temperature-dependent powder-diffraction experiments were performed *in situ* at beam line BL01C2 of National Synchrotron Radiation Research Center (NSRRC), Taiwan. X-rays of wavelength 0.77490 Å were delivered from a double-crystal monochromator with two Si(111) crystals. Samples were sealed in a quartz capillary (0.5 mm) and heated under a hot N_2 stream from 295 K to 573 K for **1a** and to 433 K for **2** during the XRD measurements. Two-dimensional PXRD patterns were recorded with an image plate detector (Mar 345, pixel size 100 μm, typical exposure duration 72 s). The distance from the sample to the image plate was 213.1094 mm; the diffraction angle was calibrated with standard Ag and Si powders. The one-dimensional (1-D) XRD profile was converted using program FIT2D (cake-type integration).

3. Results and discussion

3.1. Synthesis

The initial attempts to develop the new MOF were intended to combine the rare-earth and transition-metal ions using citric acid as the linker. From the experiments, two unknown phases were identified with powder X-ray diffraction (PXRD) and subsequently recognized as the new MOFs with novel 1D and 2D frameworks (compounds **1a** and **2**) by single-crystal X-ray diffraction.

To understand the effect of the reaction conditions to the obtained frameworks, we repeated the reactions with La^{III} or Ce^{III} ions and citric acids under varied conditions (Table 1). Two isostructural compounds **1a** and **1b** were formed in the absence of Cu^{II} ions. Like compound **2**, the obtained framework contains both citrate and oxalate ligands, indicating that the oxalate ligand was formed from the decomposition *in situ* of citric acid in the presence of Cu^{II} ions [20b,24]. Reactions performed with rare-earth nitrates (Ce^{III}/La^{III}), citric acid and oxalic acid as precursors were also attempted, but failed to deliver desired compound **2**.

According to Table 1, the deprotonated mode of the citrate ligands was found to be controlled by the hydrothermal temperature; the decomposition *in situ* of citric acid occurs only in the presence of Cu^{II} ions. Regarding the reactions of La^{III} ions, for the hydrothermal temperature 100 °C without Cu^{II} ions, only a clear solution was obtained. Facilitated with Cu^{II} ions, the citric acid decomposed *in situ*; the product was $La_2(C_2O_4)_3\cdot xH_2O$. When the hydrothermal temperature was raised to 150 °C, the title compound **1a** containing citrate ligands in three deprotonated modes was obtained regardless whether Cu^{II} ions were added. Also, in the reactions at $T=180$ °C, only the known 3D MOF phase $La(C_6H_5O_7)(H_2O)$ containing citrate ligands in one deprotonated mode was formed. For the reactions of Ce^{III} ions with citric acid, similar results were observed. The only difference was that the compound **2** was formed in the presence of Cu^{II} ions under the hydrothermal treatment at 150 °C.

3.2. Description of the structure

3.2.1. $[La_2(C_6H_5O_7)(C_6H_6O_7)(C_6H_7O_7)(H_2O)]\cdot H_2O$ (**1a**)

Compound **1** crystallized in triclinic space group $P\bar{1}$; the asymmetric unit of **1** consists of two La^{III} cations, three citric acid ligands with varied deprotonated modes, and two H_2O molecules. The formula of the title compounds is expressed as $[La_2(C_6H_5O_7)$

Table 1
Modulation of the reaction conditions.

NO.	Reagent	Metal source	Temperature (°C)	Time (h)	Product
A1	$La(NO_3)_3 \cdot 6H_2O$	N/A	100	48	Clear solution
A2	$La(NO_3)_3 \cdot 6H_2O$	N/A	150		**1a**
A3	$La(NO_3)_3 \cdot 6H_2O$	N/A	180		$La(C_6H_5O_7)(H_2O)$
B1	$La(NO_3)_3 \cdot 6H_2O$	$Cu(NO_3)_2 \cdot 3H_2O$	100		$La_2(C_2O_4)_3(H_2O)_x$
B2	$La(NO_3)_3 \cdot 6H_2O$	$Cu(NO_3)_2 \cdot 3H_2O$	150		**1a**
B3	$La(NO_3)_3 \cdot 6H_2O$	$Cu(NO_3)_2 \cdot 3H_2O$	180		$La(C_6H_5O_7)(H_2O)$
C1	$Ce(NO_3)_3 \cdot 6H_2O$	N/A	100	48	**1b**
C2	$Ce(NO_3)_3 \cdot 6H_2O$	N/A	150		**1b**
C3	$Ce(NO_3)_3 \cdot 6H_2O$	N/A	180		$Ce(C_6H_5O_7)(H_2O)$
D1	$Ce(NO_3)_3 \cdot 6H_2O$	$Cu(NO_3)_2 \cdot 3H_2O$	100		$Ce_2(C_2O_4)_3(H_2O)_x$
D2	$Ce(NO_3)_3 \cdot 6H_2O$	$Cu(NO_3)_2 \cdot 3H_2O$	150		**2**
D3	$Ce(NO_3)_3 \cdot 6H_2O$	$Cu(NO_3)_2 \cdot 3H_2O$	180		$Ce(C_6H_5O_7)(H_2O)$

$(C_6H_6O_7)(C_6H_7O_7)(H_2O)] \cdot H_2O$. The projection of **1** along the *a*-axis is shown in Fig. 1(a). Two crystallographically independent La^{III} ions form LaO_n polyhedra of two types: one is nine-coordinated and the other is ten-coordinated; the deprotonated carboxylate groups from the citrate ligand provide the donor oxygen atoms to bind to the central ion. La(1) is nine-coordinated with eight oxygen atoms belonging to carboxylate groups from five symmetry-related citric-acid molecules, and one belonging to an H_2O molecule. For each $La(1)O_9$ polyhedron, La^{III} is coordinated by O8 of a β-carboxyl group from the first (citrate)(3-) ligand, O9 of a β-carboxyl group from the second one, O1 of an α-carboxyl group, O3 of a hydroxyl group and O15 of a β-carboxyl group from the first H(citrate)(2-) ligand, O15#1 and O16 of a β-carboxyl group from the second one, O7 of an α-carboxyl group from H_2(citrate)(-) ligand, and O22 from H_2O molecule. The arrangement of these nine oxygen atoms exhibits a distorted, monocapped square antiprism as shown in Fig. 2(a). La(2) is coordinated with ten oxygen atoms of carboxylate groups also from five symmetry-related citric-acid molecules. For each $La(2)O_{10}$, La^{III} is coordinated by O9 of an α-carboxyl group, O14 of a β-carboxyl group, O12 of a hydroxyl group from the first (citrate)(3-), O14#1 and O21#1 of a β-carboxyl group from the second one, O1 of an α-carboxyl group from the first H(citrate)(2-) ligand, O2 of an α-carboxyl group from the second one, O6 of a hydroxyl group, O7 of an α-carboxyl group, and O17 of a β-carboxyl group from H_2(citrate)(-). These ten coordinated oxygen atoms form a distorted, bicapped, square antiprism as shown in Fig. 2(b). The interatomic distances of La–O vary from 2.464(3) to 2.730(3) Å, which are near those observed in several related species, such as $La(C_6H_5O_7)(H_2O)$ and $La_2(C_2O_4)_3(H_2O)_x$ [25]. Bond-valence calculations revealed that the charges of these rare-earth cations are 3.21 and 3.29 for La(1) and La(2), respectively.[26] The citrate ligands in this 1D structure are deprotonated with three coordination modes summarized in Fig. 2(c)–(e). All positions of hydrogen atoms were located and fixed from Fourier differential maps. The first citrate ligand is bound twice and adopts μ_2–η^2:η^0, μ_1–η^1:η^0 carboxyl connection modes; one hydroxyl group is connected to two La^{3+} metal-ion centers (Fig. 2(c)). The positions of hydrogen atoms were identified from the distances between C and O atoms. The interatomic distances C12–O13 and C16–O19 are larger than 1.30 Å, which is appropriate for O–H bonding. According to the description above, we conclude that the first citrate ligand is H_2(citrate)(-). The second citrate ligand contains μ_2–η^2:η^1, μ_3–η^2:η^1 carboxyl connection modes and a hydroxyl group to form a four-bound ligand (Fig. 2(d)). Taking the C–O distance into concern, only O4 is available for O-H bonding, which indicates that the second citrate ligand is H(citrate)(2-). The third citrate ligand also adopts μ_2–η^2:η^1, μ_3–η^2:η^1 carboxyl connection modes; the hydroxyl group is connected to three La^{3+} centers (Fig. 2(e)).

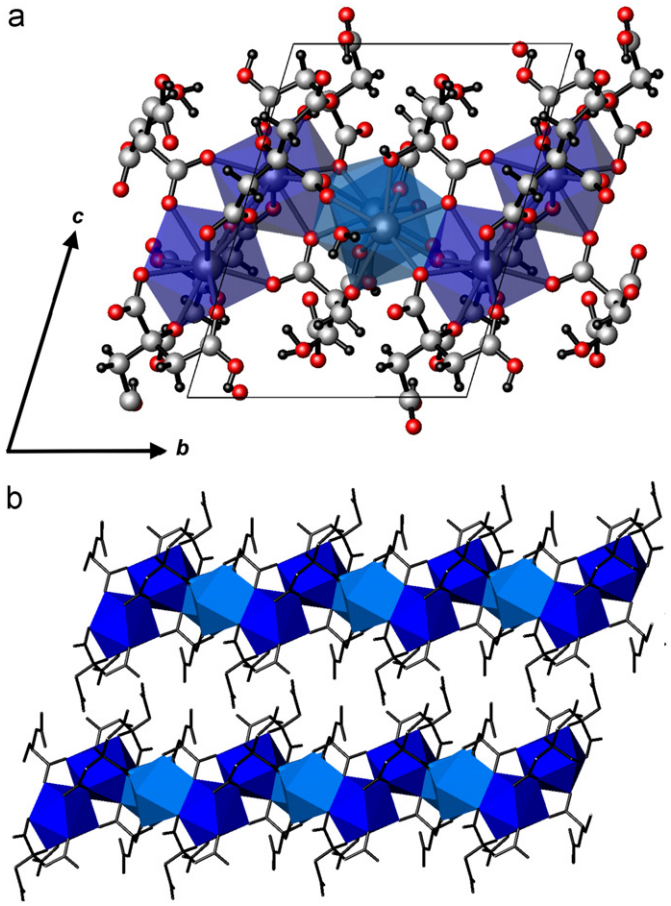

Fig. 1. (a) Crystal structure of complex **1a** viewed along the *a*-axis. Blue (light blue): La, red: O, gray: carbon, black: hydrogen; (b) 1D framework of complex **1a** projected along the *b*-axis. (For interpretation of the references to color in this figure legend, the reader is referred to the web version of this article.)

The difference from the second citrate ligand is that there is no appropriate oxygen atom to bind with a hydrogen atom. The third citrate ligand is thus (citrate)(3-). La(1) and La(2) ions are linked into two dimers through the (citrate)(3-) and H(citrate)(2-) ligands; the two adjacent (La(1))2 and (La(2))2 dimers are linked through the H_2(citrate)(-) anion to produce an edge-sharing polyhedron; the adjacent dimers are arranged alternately and expanded along the *b*-axis to form an 1D chain structure (Fig. 1(b)) in a zig-zag form. Only one compound, $Rb_2Sb_4(C_6H_5O_7)_2(C_6H_6O_7)_2(C_6H_7O_7)_4(H_2O)_2$ is known to possess a similar

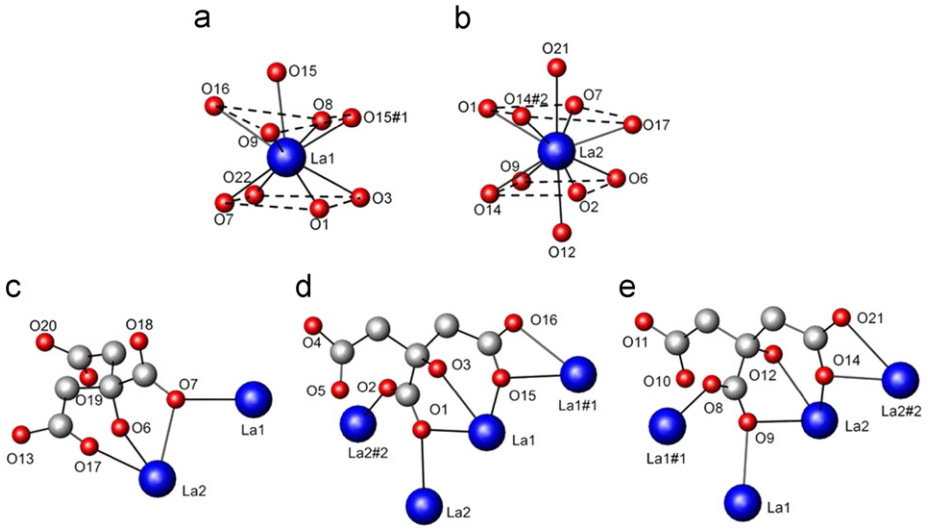

Fig. 2. (a) Coordination sphere of La(1) in **1a** forming a distorted monocapped square antiprism; (b) coordination sphere of La(2) in **1a** forming a distorted bicapped square antiprism; (c) coordination mode of citrate(3-) ligand; (d) coordination mode of H(citrate)(2-) ligand; (e) coordination mode of H_2(citrate)(-) ligand; symmetry operations: #1, $-x+1$, $-y+2$, $-z$; #2, $-x+1$, $-y+1$, $-z$.

composition and containing three separate deprotonated citric ligands [21].

3.2.2. $[Ce_2(C_2O_4)(C_6H_6O_7)_2]\cdot 4H_2O$ (**2**)

Compound **2** crystallized in monoclinic space group $P2_1/c$ (No. 14); the asymmetric unit of **2** consists of two Ce^{III} cations, two citrate ligands, one oxalate and four H_2O molecules. The structure is illustrated in Fig. 3(a); a projection of **2** along the *b*-axis is shown in Fig. 3(b). The formula is expressed as $[Ce_2(C_2O_4)(C_6H_6O_7)_2]\cdot 4H_2O$. The asymmetric unit of **2** contains one Ce^{III} cation surrounded by nine oxygen atoms from two citrate and two oxalate ligands, which form a distorted, monocapped square antiprism. The Ce^{III} ion is coordinated with nine oxygen atoms, O2 of an α-carboxyl group, O3 of a hydroxyl group, and O5 of a β-carboxyl group from the first H(citrate)(2-) ligand, O2#2 of an α-carboxyl group from the second one, O6 of a β-carboxyl group from the third one, and O7 of a β-carboxyl group from the fourth one, O1 from the first (oxalate)(2-) ligand, O4 and O4#2 from the second one. The Ce–O distances are in a range 2.46–2.69 Å, near a reported MOF with Ce^{III} ion. The bond-valence calculation for Ce atom indicates +3.10. The coordination mode of citrate and oxalate ligands is depicted in Fig. 4(b) and (c). The deprotonated citrate ligand adopts one carboxyl group in μ_1–η^1:η^0, one in μ_2–η^2:η^0, one in μ_2–η^1:η^1 connection mode and one hydroxyl group to link two adjacent Ce atoms (Fig. 4(b)). Also, O9 is bonded with a hydrogen atom, indicative of a H(citrate)(2-) ligand. Citrate ligands and Ce^{III} ions form a zigzag-type chain extending along the *b*-axis (Fig. 3(b)). The oxalate ion is six-coordinated with four Ce^{III} ions. Each CeO_9 polyhedron shares two edges and extends along the *b*-axis to form a 1D structure. The adjacent 1D chains are further connected by citrate and oxalate ligands to form a 2D network in the *bc* plane. The projection of the 2D layered structure along the *a*-axis is shown in Fig. 3(b). The layer structure of **2** contains an unbound OH group from citric acid, which is the first example of citrate and oxalate ligands to form a metal-organic coordination polymeric network. Between these (Ce) slabs, there are H_2O molecules as shown in Fig. 4. These H_2O molecules are distributed between two layer planes, which are bound to a 2D layer with hydrogen-bond interactions (Table 2).

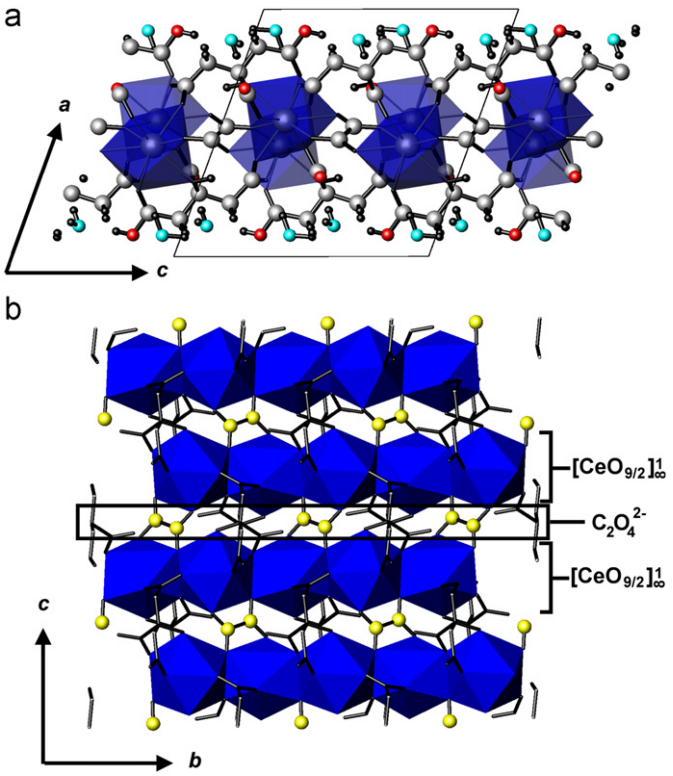

Fig. 3. (a) Crystal structure of complex **2** viewed along the *b*-axis. Blue: Ce, red: O, cyan: O of H_2O molecule, gray: carbon, black: hydrogen; (b) 2D frameworks of complex **2** in the *bc* plane. (For interpretation of the references to color in this figure legend, the reader is referred to the web version of this article.)

3.2.3. PXRD in situ

The thermal behavior of **1a** and **2** was tested using synchrotron powder X-ray diffraction *in situ* with a variable-temperature stage; the results are shown in Fig. 5(a) and (b). For compound **1a**, H_2O molecules are of two types; coordinated and uncoordinated (Fig. S2). During heating, the uncoordinated H_2O molecule became eliminated first which affected the *d*-spacing corresponding to the {100} and {001} interplanar distances. The framework

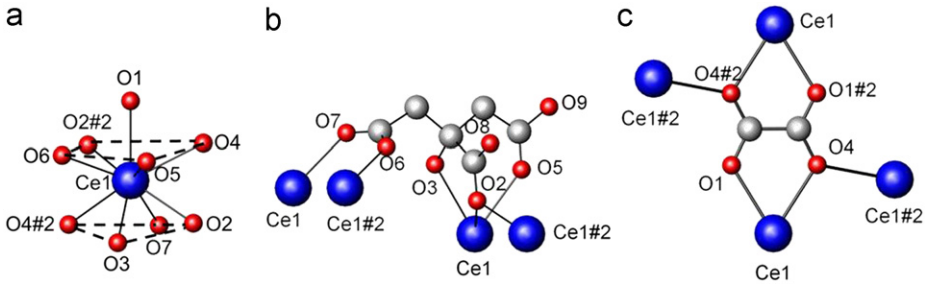

Fig. 4. (a) Coordination sphere of Ce in **2** forming a distorted monocapped square antiprism; (b) coordination mode of H(citrate)(2-) ligand; (c) coordination mode of (oxalate)(2-) ligand; symmetry operations: #1, $-x+1, y+1/2, -z+3/2$; #2, $-x+1, y-1/2, -z+3/2$.

Table 2
Crystallographic data.

Compound	**1a**	**2**
Empirical formula	$C_{18}H_{22}O_{23}La_2$	$C_7H_{10}O_{11}Ce$
Formula mass (μ)	884.18	410.27
Crystal size (mm^3)	$0.1 \times 0.2 \times 1.6$	$0.2 \times 0.4 \times 0.5$
Crystal color	Colorless	Colorless
Crystal system	Triclinic	Monoclinic
Space group	$P\bar{1}$	$P2_1/c$
T (K)	273(2)	273(2)
a (Å)	9.854(2)	12.480(3)
b (Å)	11.064(2)	8.2843(2)
c (Å)	13.508(3)	12.044(2)
α (deg.)	72.27(3)	90.00
β (deg.)	84.12(3)	109.99(3)
γ (deg.)	66.99(3)	90.00
V (Å)^3	1290.8(4)	1170.2(4)
Z	2	4
F(000)	856	792
D_{calcd} (g cm^{-3})	2.275	2.329
μ (mm^{-1})	3.373	3.946
R_{int}	0.0314	0.0526
Data/restraints/parameters	6379/0/392	2921/0/174
R_1[a], wR_2^b [$I > 2\sigma(I)$]	0.0334, 0.0649	0.0359, 0.0781
Goodness-of-fit on F^2	1.053	1.074

[a] $R_1 = \Sigma||F_o| - |F_c||/\Sigma|F_o|$; $wR_2 = [\Sigma w(F_o^2 - F_c^2)^2/\Sigma w(F_o^2)^2]^{1/2}$.

on the {100} planes exhibits a layer-like structure separated by uncoordinated water molecules, which is expected to be compressed when the uncoordinated H_2O molecules leave (Fig. S2). As for the framework on the {001} planes, the structure is rigid because of the interlayer connections from the citrate ligands; the signals related to {100} shift to a large-angle region, whereas the diffraction signal for {001} is essentially unaltered (inset in Fig. 5(a)). When the temperature was raised to ~573 K, the coordinated H_2O molecules were eliminated and the structure collapsed to form an unknown phase.

Fig. 5(b) shows the PXRD pattern *in situ* of compound **2** measured in the temperature range 333–473 K. Compound **2** possesses a layer structure stacking along direction (100) and the uncoordinated H_2O molecules are filled in two adjacent layers. On increasing temperature, the H_2O molecules are removed and the *d*-spacing of (100) decreased, which leads to the diffraction signal shifting to a larger angle, 2 theta (inset of Fig. 5(b)). The PXRD experiment *in situ* indicates that compound **2** is less stable than compound **1a**, of which decomposition begins at 433 K.

3.3. Physical properties

3.3.1. Thermogravimertic analysis

Thermogravimetric analyses (TGA) under flowing N_2 were monitored to observe the thermal behavior of **1a**, **1b**, and **2** (see Supplementary materials, Fig. S1). The TGA curves of **1a** and **1b**

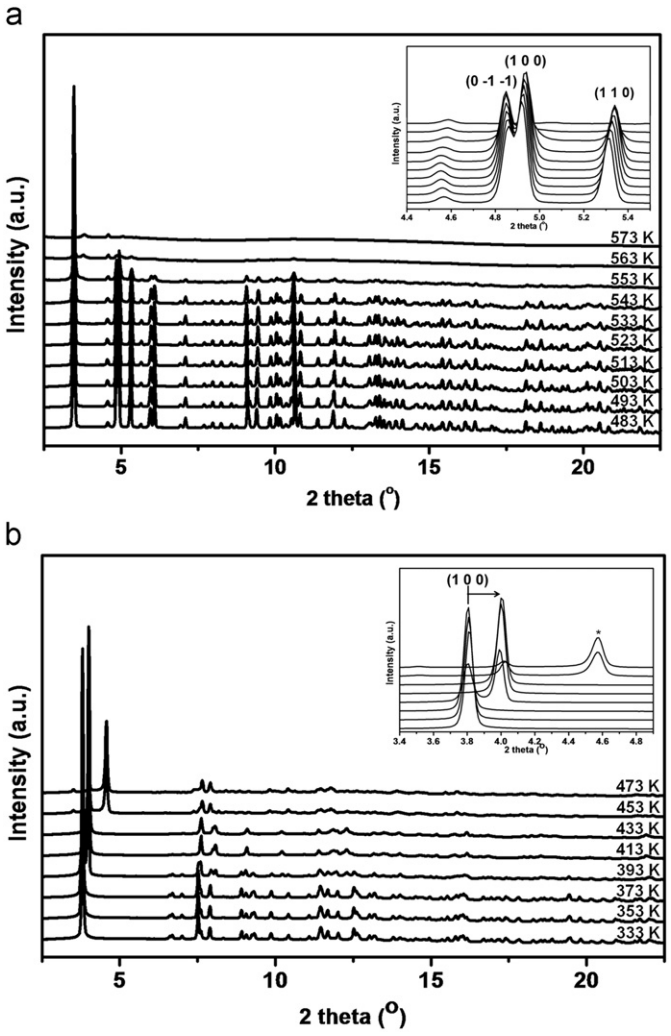

Fig. 5. Powder X-ray diffraction *in situ* of complexes **1a** (a) and **2** (b).

exhibit two obscured steps of mass loss. For compound **1a**, the curve reveals mass loss ~4% when $T < 473$ K, which corresponds to one H_2O lost (calculated 4.07%). For a temperature above 473 K, a significant loss of mass was due to the collapse of the structure, as confirmed with PXRD *in situ*. Similarly, the TGA curve of compound **1b** (dark gray line) shows a first mass loss at ~473 K; thereafter the structure collapsed. Compound **1b** began to lose mass about 473 K; a total mass loss 50.76% occurred from 473 K to 800 K, corresponding to the removal of coordinated H_2O and the combustion of the organic components (calc. 50.15%). The TGA curve of **2** reveals three steps of mass loss at temperatures near 373, 473, and 600 K. The first and second stages, occurring between 373 and

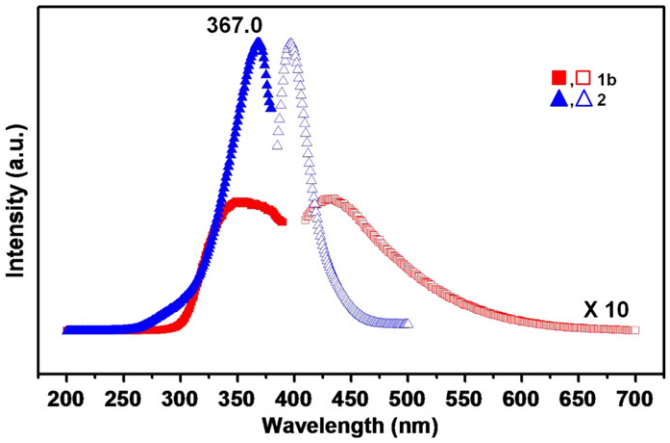

Fig. 6. Excitation and emission spectra of **1b** and **2** in the solid state.

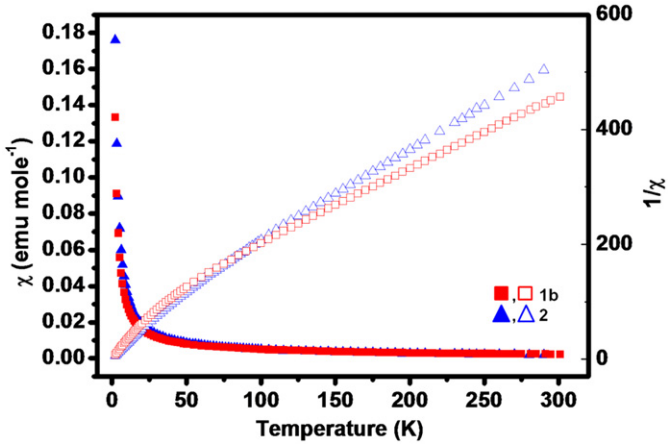

Fig. 7. Magnetic behavior depicted in the form of χT and χ^{-1} *vs.* T for **1b** and **2**.

573 K, are attributed to the loss of coordinated H_2O 8% (calc. 8.77%). The third mass loss ($T\sim600$ K) marked the initiation of structural collapse according to the PXRD *in situ*. The total mass loss 56.88% from 373 to 1000 K corresponds to the departure of coordinated H_2O and decomposition of the organic components (calc. 57.99%).

3.3.2. Photoluminescence spectra

The photoluminescence of compounds **1b** and **2** near 295 K is shown in Fig. 6. The excitation spectra (dashed line) were recorded from 200 to 400 nm to monitor the transition between the Ce^{III} $5d^1$ and $4f^1$ orbitals. Each compound shows one absorption line at 350 or 367 nm. The crystal-field splitting of the 5*d* orbital was not observed in these two complexes because of the large coordination number of Ce^{III} (9 and 10 for **1b** and 9 for **2**). Emission spectra were recorded for λ_{exc} 350 (a) and 367 (b) nm, which corresponds to excitation into the lowest energy *d*-level of Ce^{III}. The spectrum contains broad excitation bands that are assigned to a transition from the $5d^1$ excited state into two levels of the $4f^1$ ground state ($^2F_{5/2}$ and $^2F_{7/2}$).

3.3.3. Magnetic properties

Magnetic susceptibility data for all materials (Fig. 7) were measured over the temperature range 5–300 K. Data for **1b** and **2** phases follow a Curie–Weiss behavior over a wide range of temperature, with deviations observed only at low temperatures. A modified Curie–Weiss law: $\chi=\chi_0+C/(T-\theta)$, was used to fit the data; χ_0 represents the temperature-independent term, C the Curie constant, and θ the Weiss temperature. The effective moments, μ_{eff}, of **1b** and **2** are 2.45 and 2.56μ_B, respectively, which are slightly smaller than, but near, the calculated Ce^{III} moment, $\mu_{eff}=2.54\mu_B$. These values agree satisfactorily with the expected spin-only moments. The negative values of C correspond to a weak antiferromagnetic coupling between the Ce^{III} centers. The results that we found for both compounds agree satisfactorily with those found for other similar MOF with the Ce^{III} cation [18d].

4. Conclusion

We report a synthetic route to form new coordination polymers that are built from rare-earth cation and ligands of citrate and citrate/oxalate anions. Two MOF compounds, $[M(C_6H_5O_7)(C_6H_6O_7)(C_6H_7O_7)(H_2O)]\cdot H_2O$ (M=La(**1a**), Ce(**1b**)), and $[Ce_2(C_2O_4)(C_6H_6O_7)_2]\cdot 4H_2O$ (**2**) with 1D and 2D structures were synthesized. The formation of MOF with rare-earth metal ions, citrate and oxalate ligands exhibit an interesting correlation with transition-metal ion and reaction temperature. The decomposition *in situ* of citric acid in the presence of Cu^{II} ions yielded an oxalate ligand that led to the formation of **2** with a peculiar 2D structure. The synthesis of compound **2** provides a path for the preparation of further new frameworks with citrate and oxalate ligands, which deserve further investigation.

Supporting information available

X-ray crystallographic files for compounds **1a** and **2** in CIF format, TGA curves for compounds **1a**, **1b**, and **2**, and coordination tables for compounds **1a** and **2**.

Acknowledgments

We thank Dr. H.S. Sheu at National Synchrotron Radiation Research Center for technical assistance with the XRD experiment. National Science Council (NSC94-2113-M-009-012, 94-2120-M-009-014) and Center for Green Energy Technology supported this research.

Appendix A. Supplementary materials

Supplementary data associated with this article can be found in the online version at doi:10.1016/j.jssc.2012.01.046.

References

[1] (a) G.B. Gardner, D. Venkataraman, J.S. Moore, S. Lee, Nature 374 (1995) 792–795;
(b) O.M. Yaghi, M. O'Keeffe, N.W. Ockwig, H.K. Chae, M. Eddaoudi, J. Kim, Nature 423 (2003) 705–714;
(c) D. Bradshaw, T.J. Prior, E.J. Cussen, J.B. Claridge, M.J. Rosseinsky, J. Am. Chem. Soc. 126 (2004) 6106–6114;
(d) P.J. Zapf, C.J. Warren, R.C. Haushalter, J. Zubieta, Chem. Commun. (1997) 1543–1544.
[2] (a) H. Furukawa, N. Ko, Y.B. Go, N. Aratani, S.B. Choi, E. Choi, A.O. Yazaydin, R.Q. Snurr, M. O'Keeffe, J. Kim, O.M. Yaghi, Science 329 (2010) 424–428;
(b) B. Wang, A.P. Cote, H. Furukawa, M. O'Keeffe, O.M. Yaghi, Nature 453 (2008). (207-U6).
[3] (a) D.N. Dybtsev, H. Chun, S.H. Yoon, D. Kim, K. Kim, J. Am. Chem. Soc. 126 (2004) 32–33;
(b) J.L.C. Rowsell, O.M. Yaghi, J. Am. Chem. Soc. 128 (2006) 1304–1315.
[4] M. Plabst, L.B. McCusker, T. Bein, J. Am. Chem. Soc. 131 (2009) 18112–18118.
[5] (a) M. Fujita, Y.J. Kwon, S. Washizu, K. Ogura, J. Am. Chem. Soc. 116 (1994) 1151–1152;
(b) T. Sawaki, T. Dewa, Y. Aoyama, J. Am. Chem. Soc. 120 (1998) 8539–8540;
(c) J.M. Thomas, Angew. Chem.-Int. Edit 38 (1999) 3589–3628.

[6] (a) K.A. Hirsch, S.R. Wilson, J.S. Moore, Chem.-Eur. J. 3 (1997) 765–771;
(b) L. Carlucci, G. Ciani, P. Macchi, D.M. Proserpio, S. Rizzato, Chem.-Eur. J. 5 (1999) 237–243;
(c) M.A. Withersby, A.J. Blake, N.R. Champness, P. Hubberstey, W.S. Li, M. Schroder, Angew. Chem.-Int. Edit. 36 (1997) 2327–2329.
[7] (a) J. Lu, T. Paliwala, S.C. Lim, C. Yu, T.Y. Niu, A.J. Jacobson, Inorg. Chem. 36 (1997) 923–929;
(b) O.S. Jung, S.H. Park, K.M. Kim, H.G. Jang, Inorg. Chem. 37 (1998) 5781–5785;
(c) T.L. Hennigar, D.C. MacQuarrie, P. Losier, R.D. Rogers, M.J. Zaworotko, Angew. Chem.-Int. Edit. 36 (1997) 972–973.
[8] (a) R.W. Saalfrank, I. Bernt, M.M. Chowdhry, F. Hampel, G.B.M. Vaughan, Chem.-Eur. J. 7 (2001) 2765–2769;
(b) M. Du, S.T. Chen, X.H. Bu, Cryst. Growth Des. 2 (2002) 625–629.
[9] (a) L. Pan, X.Y. Huang, J. Li, Y.G. Wu, N.W. Zheng, Angew. Chem.-Int. Edit. 39 (2000) 527;
(b) S. Si, C. Li, R. Wang, Y. Li, J. Coord. Chem. 59 (2006) 215–222;
(c) N. Matsumoto, Y. Motoda, T. Matsuo, T. Nakashima, N. Re, F. Dahan, J.P. Tuchagues, Inorg. Chem. 38 (1999) 1165–1173.
[10] M.L. Tong, S. Hu, J. Wang, S. Kitagawa, S.W. Ng, Cryst. Growth Des. 5 (2005) 837–839.
[11] (a) L. Pan, M.B. Sander, X.Y. Huang, J. Li, M. Smith, E. Bittner, B. Bockrath, J.K. Johnson, J. Am. Chem. Soc. 126 (2004) 1308–1309;
(b) S.S.Y. Chui, S.M.F. Lo, J.P.H. Charmant, A.G. Orpen, I.D. Williams, Science 283 (1999) 1148–1150.
[12] (a) B.L. Chen, Y. Yang, F. Zapata, G.D. Qian, Y.S. Luo, J.H. Zhang, E.B. Lobkovsky, Inorg. Chem. 45 (2006) 8882–8886;
(b) D.L. Long, A.J. Blake, N.R. Champness, C. Wilson, M. Schroder, J. Am. Chem. Soc. 123 (2001) 3401–3402;
(c) L. Canadillas-Delgado, J. Pasan, O. Fabelo, M. Hernandez-Molina, F. Lloret, M. Julve, C. Ruiz-Perez, Inorg. Chem. 45 (2006) 10585–10594;
(d) R.S. Zhou, X.B. Cui, J.F. Song, X.Y. Xu, J.Q. Xu, T.G. Wang, J. Solid State Chem. 181 (2008) 2099–2107;
(e) P. Ayyappan, O.R. Evans, W.B. Lin, Inorg. Chem. 40 (2001) 4627–4632;
(f) X.F. Zhang, D.G. Huang, F. Chen, C.N. Chen, Q.T. Liu, Inorg. Chem. Commun. 7 (2004) 662–665;
(g) P.M. Forster, A.K. Cheetham, Angew. Chem.-Int. Edit. 41 (2002) 457–459.
[13] M. Kourgiantakis, M. Matzapetakis, C.P. Raptopoulou, A. Terzis, A. Salifoglou, Inorg. Chim. Acta 297 (2000) 134–138.
[14] W. Li, L. Jin, N.Y. Zhu, X.M. Hou, F. Deng, H.Z. Sun, J. Am. Chem. Soc. 125 (2003) 12408–12409.
[15] M. Dakanali, E.T. Kefalas, C.P. Raptopoulou, A. Terzis, T. Mavromoustakos, A. Salifoglou, Inorg. Chem. 42 (2003) 2531–2537.
[16] G.Q. Zhang, G.Q. Yang, J.S. Ma, Cryst. Growth Des. 6 (2006) 375–381.
[17] (a) N. Kotsakis, C.P. Raptopoulou, V. Tangoulis, A. Terzis, J. Giapintzakis, T. Jakusch, T. Kiss, A. Salifoglou, Inorg. Chem. 42 (2003) 22–31;
(b) M. Murrie, S.J. Teat, H. Stoeckli-Evans, H.U. Gudel, Angew. Chem.-Int. Edit. 42 (2003) 4653–4656.
[18] (a) R. Baggio, M. Perec, Inorg. Chem. 43 (2004) 6965–6968;
(b) S.G. Liu, W. Liu, J.L. Zuo, Y.Z. Li, X.Z. You, Inorg. Chem. Commun. 8 (2005) 328–330;
(c) F.Y. Li, L. Xu, G.G. Gao, L.H. Fan, B. Bi, Eur. J. Inorg. Chem. (2007) 3405–3409;
(d) R.S. Zhou, J.F. Song, Q.F. Yang, X.Y. Xu, J.Q. Xu, T.G. Wang, J. Mol. Struct. 877 (2008) 115–122.
[19] (a) S. Romero, A. Mosset, J.C. Trombe, J. Solid State Chem. 127 (1996) 256–266;
(b) B. Chapelet-Arab, G. Nowogrocki, F. Abraham, S. Grandjean, J. Solid State Chem. 177 (2004) 4269–4281;
(c) C. Gabriel, C.P. Raptopoulou, C. Drouza, N. Lalioti, A. Salifoglou, Polyhedron 28 (2009) 3209–3220.
[20] (a) E. Asato, W.L. Driessen, R.A.G. Degraaff, F.B. Hulsbergen, J. Reedijk, Inorg. Chem. 30 (1991) 4210–4218;
(b) M.S. Grigoriev, C. Den Auwer, D. Meyer, P. Moisy, Acta Crystallogr. Sect. E-Struct. Rep. Online 62 (2006) M1725–M1727.
[21] R.C. Bott, G. Smith, D.S. Sagatys, D.E. Lynch, C.H.L. Kennard, Aust. J. Chem. 53 (2000) 917–924.
[22] Siemens Analytical X-ray Instruments Inc., Madison, WI, USA, 2001.
[23] (a) G.M. Sheldrick, 1997;
(b) Reference Manual, Siemens Analytical X-Ray Systems, Inc, Madison, WI, USA, 1996, 2000.
[24] X.M. Zhang, Coord. Chem. Rev. 249 (2005) 1201–1219.
[25] (a) A. Michaelides, S. Skoulika, A. Aubry, Mater. Res. Bull. 23 (1988) 579–585;
(b) H. Shenghua, Z. Gongdu, T.C.W. Mak, J. Crystallogr. Spectrosc. Res. 21 (1991) 127–131.
[26] L.D. Brown, D. Altermatt, Acta Crystallogr. B 41 (1985) 244.